Breakup of an electrified, perfectly conducting, viscous thread in an AC field

D. T. Conroy, O. K. Matar, R. V. Craster, and D. T. Papageorgiou

Phys. Rev. E **83**, 066314 — Published 17 June 2011

DOI: 10.1103/PhysRevE.83.066314

Breakup of an electrified, perfectly conducting, viscous thread in an AC field

D. T. Conroy,[1] O. K. Matar,[1] R. V. Craster,[2] and D. T. Papageorgiou[2]
[1)] *Department of Chemical Engineering,*
Imperial College London, South Kensington Campus, London, SW7 2AZ, U.K.
[2)] *Department of Mathematics,*
Imperial College London, South Kensington Campus, London, SW7 2AZ, U.K.

We study the axisymmetric break-up and satellite formation of slender jets surrounded by a concentrically-placed cylindrical electrode and subjected to time-dependent AC electric fields. The jet is assumed to be a perfectly conducting viscous fluid and surrounded by a dielectric inviscid gas. We use the long-wave approximation to derive coupled evolution equations for the interface position, and axial velocity component, which accounts for electrostatic forcing. The electrostatic force in this case is large and competes with capillary forces near the rupture point, causing the interface to oscillate and the satellite to have shapes that are distinct from the DC case. In particular, our results indicate that it may be possible to use the AC field to control the number of satellites accompanying breakup as well as their size.

I. INTRODUCTION

The breakup of electrified jets has been extensively studied by many investigators[1–10] as a way of controlling the droplet size in applications such as electrospraying, electro separations, electrospray mass spectrometry and ink-jet printing. Electric fields are also used to stabilize drawn fibres for electro-spinning applications in order to make micro-threads for the textile industry.

A considerable amount of work on electric free jets has been performed since the work of Rayleigh[11] in which a sufficiently large wavelength perturbation causes the jet to break up into droplets as a result of capillary forces. As jet drainage evolves towards rupture, capillary forces and velocities become very large and numerical methods are required to capture the dynamics. Numerical results have been performed in the Stokes flow limit by Pozrikidis[12] using boundary integral methods and by Wilkes, Phillips and Basaran[13] using finite-element methods for the full Navier-Stokes equations. Further, numerical solutions to one-dimensional approximations, derived in the long-wave limit have been used by many researchers[14–16] with good agreement with the full solution and experiments[13]. The equations associated with this approach are easier to solve numerically with high accuracy, whilst accounting for the dominant physics near break-up. For this reason, the long-wave approximation will be investigated in this paper.

In the presence of radially-applied electric fields, an additional Maxwell stress acts on the fluid, and for leaky-dielectrics, this force acts on the interface[17]. For perfectly conducting liquid threads, the voltage potential is fixed and the electrostatic stress acts only normal to the interface with the electric field arising from the annular layer. In this case, the electrostatic pressure has a stabilizing effect for long wavelengths and a destabilizing effect for short wavelengths[5]. For perfectly conducting viscous threads surrounded by a dielectric inviscid gas, numerical solutions for two-dimensional models have been performed by Collins, Harris and Basaran[7] and one-dimensional models by López-Herrera and Gañán-Calvo[9], Collins, Harris and Basaran[7], López-Herrera, Gañán-Calvo and Perez-Sabroid[18] and Wang, Mahlmann and Papageorgiou[10]. Experimentally, the effect of electric field strength on the satellite size and charge was investigated by López-Herrera and Gañán-Calvo[9]. They also found reasonably good agreement with their one-dimensional model for moderate electric field strengths.

In this paper, we investigate perfectly conducting fluids in radially-applied AC electric fields. Linear theory for this time dependent problem was investigated by González, García and Castellanos[19] for the one dimensional model, using a Floquet analysis. They found that for large-wavelength perturbations in an AC field, for constant parameter values, the jet becomes more unstable with increasing wavenumber to a critical value and then the electrostatics is stabilizing. The stability of liquid films in AC fields was also investigated by Roberts and Kumar[20] using both a Floquet analysis for the linear problem and numerically to study how electric effects can be used to control topological features. Currently, electrified jets in AC fields have not been investigated to study the dynamics near breakup. Since AC fields could potentially be useful in controlling satellite size and shape, we study this problem here.

The rest of the paper is organized as follows: in section II, the model is formulated for a perfectly conducting fluid and reduced asymptotically for long wavelengths. In section III, we solve the governing equations numerically, discussing the results and finally in section IV provide concluding remarks.

II. FORMULATION

We consider two immiscible fluids in a core-annular arrangement, bounded by a concentric, cylindrical electrode of radius R_2. An interface separating the two fluids is located at $r = S(z,t)$ (axisymmetric flows are studied here) with initial radius R_0 and surface tension γ. The annular fluid is an inviscid dielectric with permittivity ε_2, whereas the core fluid is a perfect conductor with density ρ_1, viscosity μ_1 and potential $\phi_s = 0$. At the wall, a time-dependent potential, $\phi_w = A\cos(\omega t)$, is applied

where A is the amplitude and ω is the frequency. Gravity is ignored and an axisymmetric geometry is assumed throughout, with cylindrical polar coordinates (r, z) and corresponding velocity field (u, w).

A. Governing equations

The formulation of the model follows Saville[17], with the equations non-dimensionalized as follows: r and S are scaled on the initial thread radius, R_0, the axial length z on a scale L, the radial velocity on γ/μ_1, axial velocity on $\delta^{-1}\gamma/\mu_1$, time on $R_0\mu_1/\gamma$, pressure with γ/R_0 and the electric field as A/R_0 (where A is the amplitude of the wall potential). The parameter δ is a slenderness ratio defined by $\delta = R_0/L$.

In dimensionless form, the momentum and continuity equations in the core are given by

$$Re\left(u_t + uu_r + wu_z\right) = -p_r + u_{rr} + \frac{1}{r}u_r + \delta^2 u_{zz} - \frac{u}{r^2}, \tag{1}$$

$$Re\left(w_t + uw_r + ww_z\right) = -\delta^2 p_z + w_{rr} + \frac{1}{r}w_r + \delta^2 w_{zz}, \tag{2}$$

$$\frac{1}{r}\left(ru\right)_r + w_z = 0, \tag{3}$$

with subscripts denoting partial derivatives. Here, the dimensionless group appearing in the momentum equation is

$$Re = \frac{\rho_1\gamma R_0}{\mu_1^2}, \tag{4}$$

and represents the Reynolds number. Note also that $Re = Oh^{-2}$ where Oh is the Ohnesorge number that measure the ratio of viscous forces to inertial and surface tension forces - large values of Oh represent flows with significant surface tension, as is the case in the present study. The velocity field $\mathbf{u}$ at the axis must be bounded, and this supplies one of the conditions required to solve the problem. The other conditions come from a balance of forces at the interface discussed below. We will need the vectors $\mathbf{n} = (1, -S_z)/(1+S_z^2)^{1/2}$, $\mathbf{t} = (S_z, 1)/(1+S_z^2)^{1/2}$ which are the unit normal (pointing outwards) and tangent at any point on the interface. Note: Regions 1 and 2 represent the core and annulus, respectively.

The voltage potential in the annular layer is determined by Laplace's equation (the corresponding electric field is given by $\mathbf{E} = -\nabla\phi$):

$$\frac{1}{r}\left(r\phi_r\right)_r + \delta^2\phi_{zz} = 0, \tag{5}$$

with the boundary conditions $\phi(R_2, z, t) = \cos(\omega t)$ and $\phi(S, z, t) = 0$. The latter condition follows because the core fluid is perfectly conducting and without loss of generality is taken to be at zero potential. The derivation of equation (5) is presented in the appendix, where we have also justified the neglect of magnetic fields for the sufficiently small voltage potentials and frequencies studied here. Note also that the local surface charge density, $q_s(z,t)$ say, can be calculated from Gauss's law once the electric potential ϕ is determined. Hence we have (at $r = S(z,t)$),

$$\epsilon_2\mathbf{E}\cdot\mathbf{n} = q_s, \quad \text{or} \quad q_s = -\epsilon_2\frac{\partial\phi}{\partial n}, \tag{6}$$

where q_s has been non-dimensionalized by $\epsilon_0 A/R_0$, and ϵ_2 is the relative permittivity of region 2 with respect to that of air defined by ϵ_0, say. Written out in full, equation (6) reads

$$q_s(z,t) = -\epsilon_2(\phi_r - \delta^2 S_z\phi_z)/(1+\delta^2 S_z^2)^{1/2}. \tag{7}$$

At the interface, the fluid stress comes from the core region 1 and the electrostatic stress comes from the annular region 2, so the normal and tangential stress balances are

$$p - \frac{1}{1+\delta^2 S_z^2}\left(u_r - \delta S_z(\delta u_z + \delta^{-1}w_r) + \delta^2 S_z^2 w_z\right) + \frac{\varepsilon_2 E_b}{2}\frac{1-\delta^2 S_z^2}{1+\delta^2 S_z^2}((\phi_{2r})^2 - \delta^2(\phi_{2z})^2) - \frac{2\delta^2\varepsilon_2 E_b S_z}{1+\delta^2 S_z^2}\phi_{2r}\phi_{2z} = \kappa = \left(\frac{1}{S(1+\delta^2 S_z^2)^{1/2}} - \delta^2\frac{S_{zz}}{(1+\delta^2 S_z^2)^{3/2}}\right), \tag{8}$$

$$\left(u_r S_z + \frac{1}{2}(1-\delta^2 S_z^2)(u_z + \delta^{-2}w_r) - S_z w_z\right) = 0, \tag{9}$$

respectively. Here $\kappa = \nabla\cdot\mathbf{n}$ is the curvature and

$$E_b = \frac{\varepsilon_0 A^2}{\gamma R_0} \tag{10}$$

is the electrostatic Webber number relating electrostatic to capillary forces. Finally, the dimensionless kinematic condition is

$$S_t + w_1 S_z = u_1. \tag{11}$$

B. Reduced model

The evolution equations for an electrified jet using the long-wave assumption have been derived previously in[7,10], the only difference being that we essentially make the electrostatic Weber number time-dependent. Following these approaches we re-derive the one-dimensional model by making the long-wave approximation[14,23], and assuming $\delta \ll 1$. In order to keep inertia, we balance inertial and capillary forces so that $Re = \delta^2\bar{Re}$. The annular fluid is assumed to be inviscid but it is sufficient to assume that the viscosity and density of the core fluid is much larger than that of the annular fluid so that the

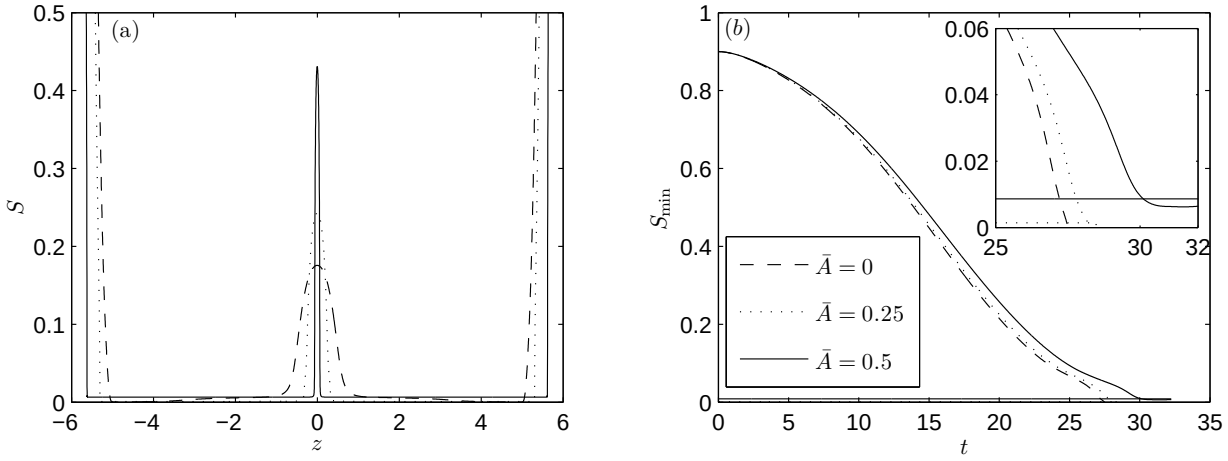

FIG. 1. Results for the DC case ($\omega = 0$) showing the effect of varying $\bar{A}$: (a) the satellite shape near rupture and (b) the evolution of the minimum interface height. In panel (b), the insert in the upper right-hand corner is a magnification of the region near breakup in (a), with the horizontal lines (line types here go with the $S_{\min}$ lines) indicating the interface height where capillary and electrostatic forces balance. Also, the satellite volumes are $V = 0.0695, 0.066$ and 0.053 for $\bar{A} = 0, 0.25$ and 0.5 respectively and $R_2 = 10$.

stress from the annular region is a higher order contribution. We adopt the expansion $u = u_0 + \delta^2 u_1 + ...$ for the velocity and similar expansions for the other variables. In the core, the axial momentum equation to leading order yields, after integration and applying the boundary conditions, $w_0 = w_0(z,t)$ and using the continuity condition the radial velocity is $u_0(r,z,t) = -rw_{0z}/2$. The radial momentum equation to leading order, after integrating w.r.t. r, is $p_0 = p_0(z,t)$ and the axial momentum equation to first order, after integrating w.r.t. r, is

$$w_1 = \frac{r^2}{4}\left[\bar{Re}(w_{0t} + w_0 w_{0z}) - w_{0zz} + p_{0z}(z,t)\right] + F(z,t), \tag{12}$$

where $F(z,t)$ is a function that is determined in terms of $S(z,t)$ in the analysis. The pressure is found from the leading order normal stress balance and is

$$p_0 = -\frac{E_b \varepsilon_2}{2}\left(\phi_{0r}\right)^2\big|_{S_0} - w_{0z}|_{S_0} + \kappa, \tag{13}$$

where S_0 is the leading order surface position. Combining equation (12) with the tangential stress balance to leading order, given by

$$-3S_{0z}w_{0z} - \frac{S_0}{2}w_{0zz} + w_{1r} = 0, \tag{14}$$

yields the following evolution equation for the axial velocity

$$\bar{Re}(w_{0t} + w_0 w_{0z}) = \frac{2}{S_0}\left(3S_{0z}w_{0z} + \frac{3}{2}S_0 w_{0zz}\right) - \kappa_z + \frac{1}{2}E_b\left(\varepsilon_2\left(\phi_{0r}\right)^2\big|_{S_0}\right)_z. \tag{15}$$

Here we have kept the full curvature term[15] because the higher order term acts as a regularization condition by providing a short wavelength cut-off. Further, we do not retain the higher order term multiplying the electrostatic contribution, found in López-Herrera, Gañán-Calvo and Perez-Sabroid[18], because it remains small for the long wavelengths studied here. We have checked that this is true for our numerical results and that including this term does not have a significant effect on the surface position or evolution of the minimum interface height. The potential in the annular region is

$$\phi_0 = \phi_w - \phi_w \frac{\log(r/R_2)}{\log(S_0/R_2)}, \tag{16}$$

where $\phi_w = \cos(\omega t)$. From this equation and (6) the surface charge is $q_s = \varepsilon_2 \phi_w / S_0 \log(S_0/R_2)$.

The leading order axial velocity, after rescaling as $S_0 \to \bar{Re} S$, $t \to \bar{Re}\, t$, $w_0 \to \bar{Re}^{-1} w$, $\omega \to \bar{Re}^{-1}\omega$ and $R_2 \to \bar{Re}\, R_2$, to absorb the Reynolds number, is determined from the solution of the following evolution equations

$$w_t + w w_z = \frac{3}{S^2}\left(S^2 w_z\right)_z - \kappa_z + \left(\frac{\bar{\phi}_w^2}{(S\log(S/R_2))^2}\right)_z, \tag{17}$$

$$S_t + wS_z + \frac{S}{2}w_z = 0, \tag{18}$$

with $\bar{\phi}_w = \bar{A}\cos(\omega t)$ and $\bar{A} = \sqrt{E_b \varepsilon_2 / 2\bar{Re}}$.

III. RESULTS

Since the linear stability problem has been investigated elsewhere our aim is to investigate the nonlinear dynamics. The governing equations are solved using PDECOL[24], which is based on the method of lines with

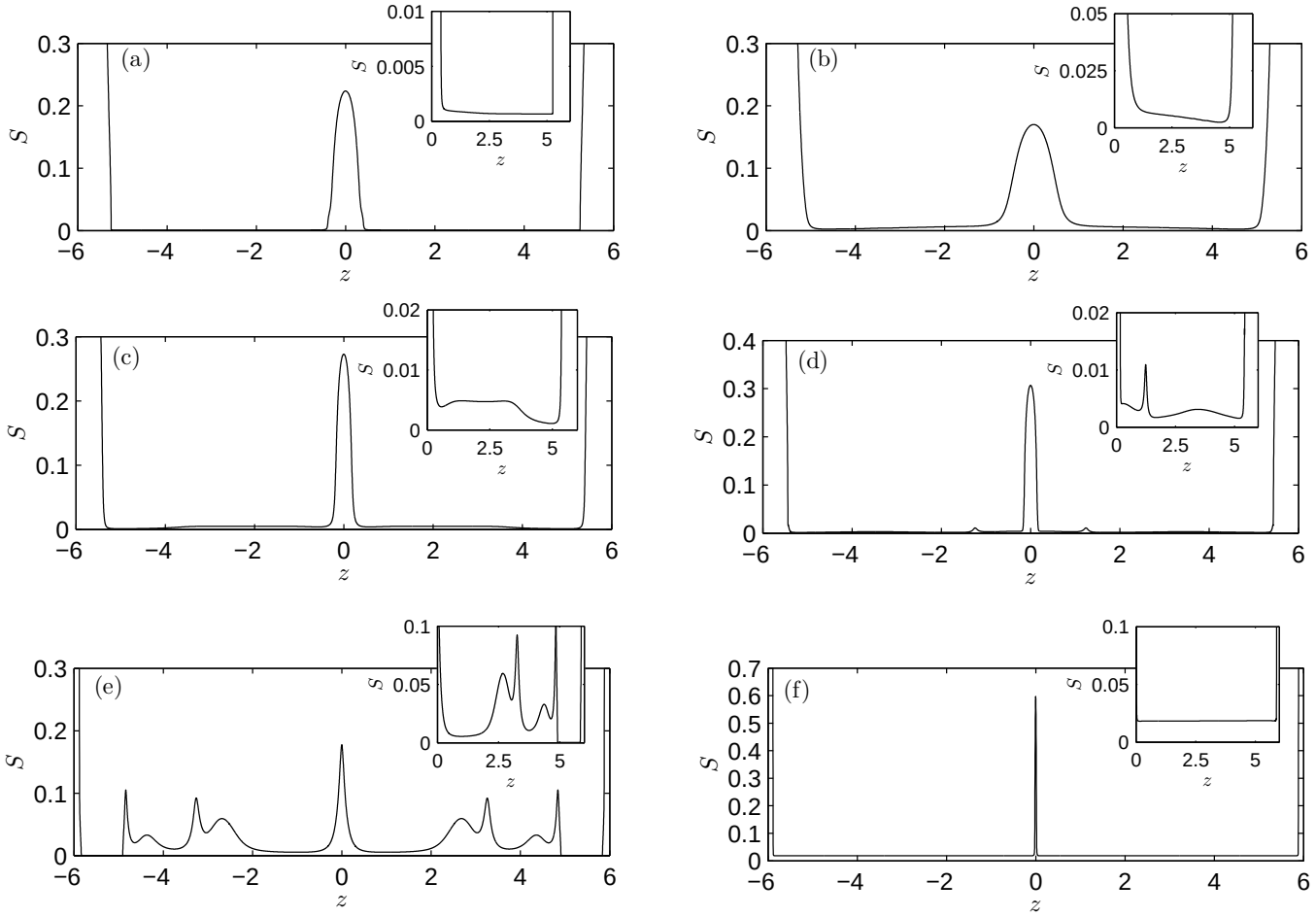

FIG. 2. Results for the AC case showing the satellite shape near rupture for $\omega = 1$ (left hand panels) and $\omega = 10$ (right hand panels). In panels (a) through (f), the inset in the upper right-hand corner is a magnification of the region near breakup and in all cases $R_2 = 10$. Also, the satellite volumes are $V = 0.0674, 0.062$ and 0.042 ($\omega = 1$) and $V = 0.0675, 0.0616$ and 0.0263 ($\omega = 10$) for $\bar{A} = 0.25$ (panels a and b), 0.5 (panels c and d) and 1 (panels e and f) respectively.

space discretized using finite element collocations. Typically, $8,000$ grid points were used and the equations were solved on the domain $-L \le z \le L$, with $L = 2\pi$.

The following initial conditions, corresponding to a perturbation in the film height, are used:

$$w(z,0) = 0, \tag{19}$$

$$S(z,0) = 1 - 0.1\cos(kz), \tag{20}$$

where $k = 2\pi/L$ is the wave number and the periodic boundary conditions are

$$w(-L,t) = 0, \quad w(L,t) = 0, \tag{21}$$

$$S_z(\pm L,t) = S_{zzz}(\pm L,t) = 0. \tag{22}$$

We set $\delta = 0.01$, which is consistent with previous work[23], and note that the wavenumber k is dimensionless, scaled by $R_0\delta$. We have validated our numerical results against linear theory in the DC case, checked that the total mass of the fluid is conserved for each run and checked numerically that the next order term $\delta^2 S_z^2 \ll 1$ as break up is approached.

For $\bar{A} \gg 1$ numerical results (not shown here) indicate that the interface is stable to perturbations at all frequncies, which is also consistent with results from the stability analysis, found in equation (23), for DC fields and the electrode radius investigated here[25]. For intermediate values of $\bar{A}$ the interface oscillates with the AC field, thinning the neck and pulling the swell towards the electrode signaling wall touchdown singularities[10], and the code generally halts. For this reason we limit our parameter space to $\bar{A} \le 1$. In all cases the electrode radius has been set to $R_2 = 10$, which ensures that the swell never makes contact with the wall. Variations in R_2 do not have a significant effect on the results and has been fixed to this value by others[7]. Further, as $S \to 0$ the capillary terms behave as S^{-2}, whereas the electrostatic terms behave as $-2\phi_w^2 S^{-3}(\ln(S/R_2))^{-2}$ and therefore have the opposite sign. In the absence of electrostatic

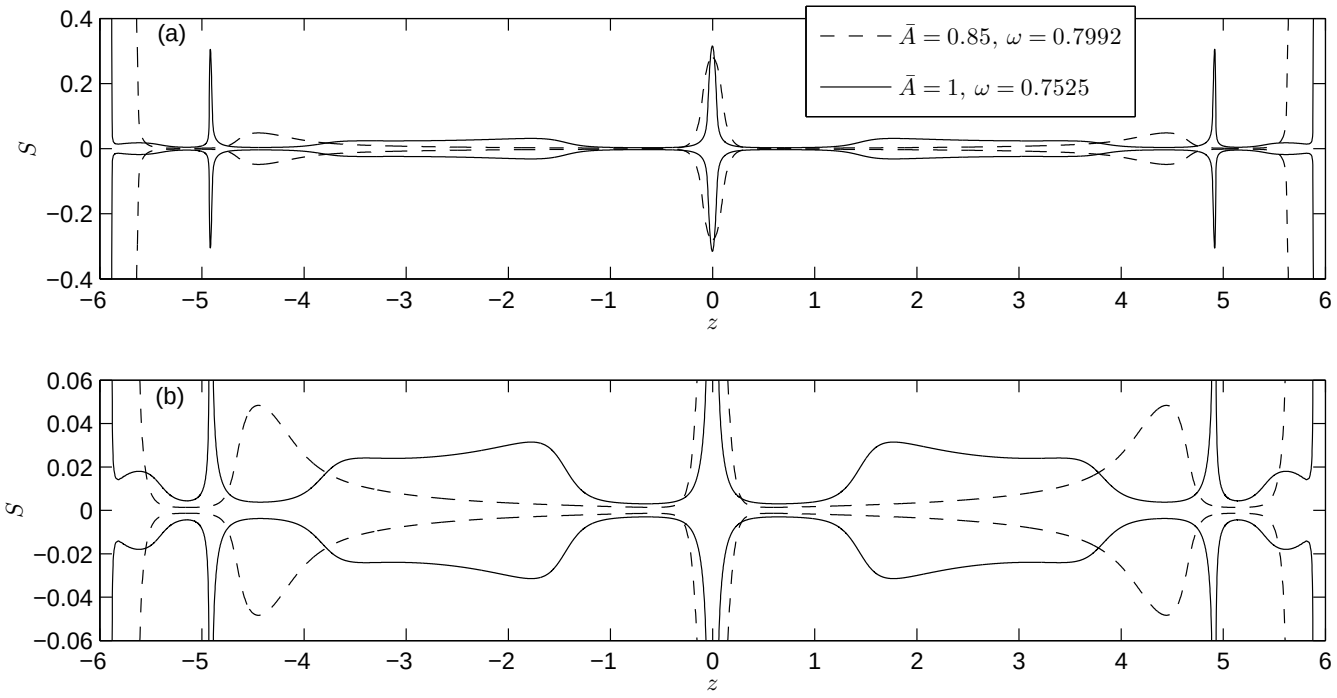

FIG. 3. Surface position near rupture, showing the formation of possibly three and five satellites; panel (b) is a magnification of panel (a). Here $R_2 = 10$ for both panels and the plots are taken at $t = 33.4$ (solid line) and $t = 39.6$ (dashed line). For $\bar{A} = 0.85$ the volume for the central, sub and total (sum of all) satellite drops are: $V = 0.0406$, $V = 0.0042$ and $V = 0.049$ respectively. For $\bar{A} = 1$ the volume for the central, sub1 (closest to the central one), sub2 and total (sum of all) satellite drops are: $V = 0.02$ and $V = 0.0053$, $V = 0.0065$ and $V = 0.0435$ respectively. Note that the thread is axisymmetric and in this figure we have included $\pm S$.

forces, the scaling of Eggers[15] holds near breakup but for strong electric effects the similarity solution is unknown[7]. We can argue that if the electric Webber number is sufficiently weak, then the interfacial height at which electrostatic forces become important will be smaller than we can obtain numerically. In this case the fluid dynamic ($E_b = 0$) scaling will hold. Of course, at very small interfacial heights other forces, such as van der Waals and electrokinetic, will be important, but we will assume that these are much weaker than the electrostatic forces investigated here. Further, the electrostatic force is oscillating in time so there will be periods at which capillary forces dominate. Therefore, for small frequencies ω we expect the fluid dynamic scaling to hold in some cases.

A. Direct current (DC) case

For the DC case, we can derive the dispersion relation by expanding equations (17) and (18) about the base state, e.g. $w = 0 + \hat{w}$, $S = 1 + \hat{S}$, with $(\hat{w}, \hat{S}) = (w', S') \exp(\lambda t + ikz)$, to obtain

$$\lambda^2 + 3k^2\lambda - \frac{1}{2}k^2\left(1 - \delta^2 k^2\right) + \bar{\phi}_w^2\left(\frac{\ln(R_2) - 1}{\ln(R_2)^3}\right)k^2 = 0. \tag{23}$$

This is the form found in Wang, Mahlmann and Papageorgiou[10], obtained directly from the one-dimensional model and the full dispersion relation, for Stokes flow, in the long wave limit. From this equation it is evident that electrostatics is stabilizing for $\ln(R_2) > 1$ and destabilizing otherwise.

A comparison of the satellite shape as a function of effective wall potential in the DC case is displayed in Figure 1. A satellite is defined to be the region between both rupture points at the location of $S_{\min}$ and may in principle contain multiple satellites. Increasing $\bar{A}$ causes the satellite to become more disk like with an increasing radial extent and thinner in the z direction. This result was also found by Collins *et al.*[7] for increasing electric field strength and as noted by them, the disk maybe the formation stage of the fine jet that was observed experimentally by Cloupeau and Prunet-foch[26]. Since the electrostatics has a stabilizing effect, as indicated from linear theory, the rupture time naturally increases with $\bar{A}$ and for very large electrostatic effects the interface may ac-

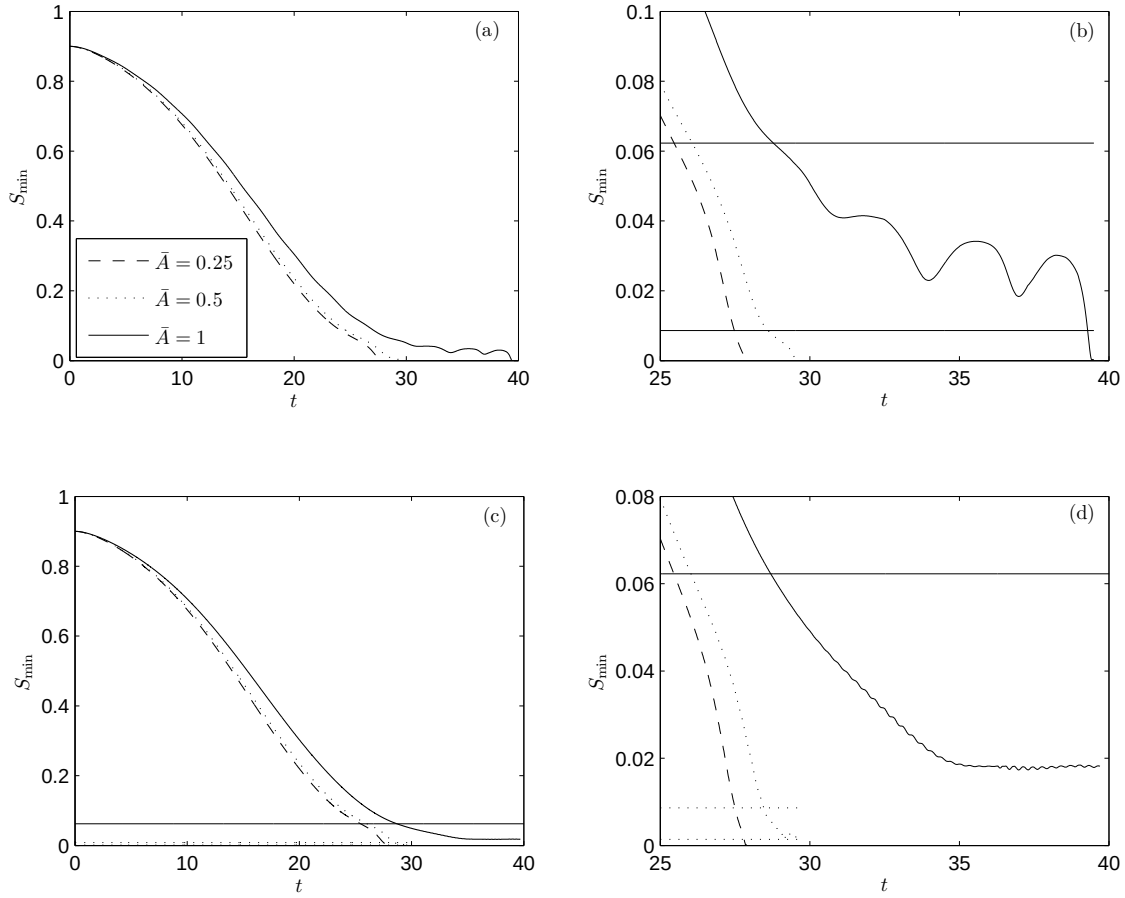

FIG. 4. Results for the AC case showing the evolution of the minimum interface height for $\omega = 1$ (panels a and b) and $\omega = 10$ (panels c and d). In the upper right-hand corner is a magnification of the region near breakup, with the horizontal lines (line types here go with the $S_{\min}$ lines) indicating the interface height where capillary and electrostatic forces balance at $\bar{A}$ and $\bar{A}/2$ (time averaged value). In all cases $R_2 = 10$.

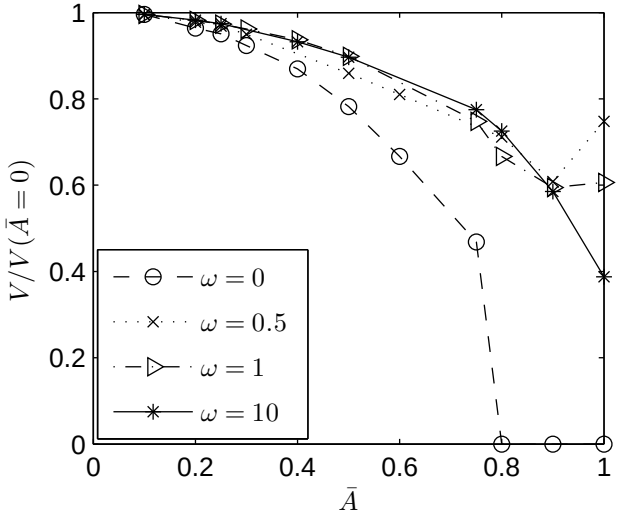

FIG. 5. Satellite volume, scaled by that obtained in the absence of electric fields, near rupture as a function of frequency, ω, and amplitude $\bar{A}$ with $R_2 = 10$.

tually arrest at some position[10]. This position correlates with the location where electrostatic and capillary pressures balance as shown by the horizontal lines in Figure 1. For intermediate values of $\bar{A}$, shown in the figure, a stable microthread forms but a satellite is also present that continues to rise in the centre.

B. Alternating Current (AC) case

The satellite structure in the AC case for two different driving frequencies is shown in Figure 2. The results are sensitive to the frequencies because a large part of the dynamics depends on whether or not the oscillating electrostatic pressure is strong or weak near the rupture point. For large values of $\bar{A}$, the disk-like satellite structure forms, as in the DC case, although it is not as long or thin owing to the reduced strength of the electric field averaged over time. Also, in the AC case, the interface does not taper smoothly to the rupture point but has a lobed structure, with more lobes appearing as $\bar{A}$ increases.

For a suitable choice of parameter values, the interface appears to rupture at multiple points as indicated in Figure 3. The frequency in these plots has been tuned in order to obtain a minimum interface hight at multiple locations. The number of pinching points increases with the strength of the electric field and may promote multiple satellite-formation. In all of these cases, assuming that pinching occurs at all the minimum heights, the central satellite (near $z = 0$) is the largest but for the $\bar{A} = 1$ case this volume is only 46% of total volume of all satellites. Therefore, the AC field may be useful in decreasing the total satellite volume by promoting the formation of multiple satellites.

The evolution of the minimum interface height is shown in Figure 4 and, similarly to the DC case, the electric field acts to slow the time to rupture. For small times, the capillary forces dominate and the interface does not oscillate noticeably with the AC field. As the interface height S decreases, however, the electrostatic term grows relative to the capillary terms and the interface oscillates with the electric field. The oscillation appears to be bounded between the value of $S(z,t)$ where capillary forces balance electrostatic forces at the maximum and time-averaged squared wall potential (see Figure 4 insert). The time-average position of the interface decreases and eventually reaches a point where the rupture time scale is faster than the period of the AC field and the jet ruptures. For large values of $\bar{A}$ a stable, although oscillating, microthread appears but with a very long satellite as in the DC case.

The key difference between AC and DC fields is highlighted in Figure 5 where the satellite volume (given here in dimensionless form as $V = \pi \int S^2 \mathrm{d}z$) is plotted as a function of frequency for different amplitudes. For the DC case, the satellite volume decreases with electrostatic strength, in contrast to Collins *et al*[7] who found the satellite volume to increase; the different trends may be due to the fact that we are investigating much larger wavelengths. Our trend, however, was also found for inviscid jets[27] when the wavenumber was smaller than a critical value. For large frequencies, the oscillation of the wall potential is fast relative to the drainage time and the AC field acts as an effective DC field, with a smaller time averaged potential, that causes the volume to be smaller than the DC case. For small frequencies, the drainage time scale is fast relative to the oscillation period of the wall potential, and the strength of the electric field near the rupture time is sensitive to the chosen parameter values. As a result the satellite volume can be sensitive to $\bar{A}$ and ω and this is the reason for the rise in the volume near $\bar{A} = 1$ ($\omega = 0.5$ and 1).

IV. CONCLUSION

This study has investigated the break-up of perfectly conducting viscous threads, surrounded by a hydrodynamically passive annular region, in the presence of an AC electric field applied by a concentric electrode. The governing equations were asymptotically reduced in the slender long-wave limit and the resultant equations were solved numerically. Since the core fluid is a perfect conductor, the electrostatic force competes with capillary forces near rupture, and the AC field has an important effect on the evolution of the thread radius and shape of the final satellite. For sufficiently strong wall potential amplitudes, the interface oscillates with the electric field near the point where capillary and electrostatic forces balance. As in the DC, case a disk-like satellite forms but with a larger volume, and smaller radius, due to the weaker electrostatic force averaged over time. Further, the main central satellite does not taper smoothly to the rupture point but has a lobed structure with the possibility of forming multiple satellites. In any event, these results are suggestive that AC fields could be used to control the number and size of satellites, giving one more degree of reedom than a purely DC field.

Appendix A: Justification of the electrostatic limit for AC fields

Here we explore the validity of the electrostatic model and identify AC frequencies for which our results are expected to hold. We start with Maxwell's equations in dimensional form

Gauss′s Law	$\nabla \cdot (\epsilon \mathbf{E}) = q$	(A1)
Faraday′s Law	$\nabla \times \mathbf{E} = -\mu \dfrac{\partial \mathbf{H}}{\partial t}$	(A2)
No magnetic charges	$\nabla \cdot \mathbf{H} = 0$	(A3)
Magnetic induction	$\nabla \times \mathbf{H} = \mathbf{J} + \epsilon \dfrac{\partial \mathbf{E}}{\partial \mathbf{t}}$	(A4)
Charge conservation	$q_t + \nabla \cdot \mathbf{J} = 0$	(A5)
Current constitutive law	$\mathbf{J} = \sigma \mathbf{E} + q\,\mathbf{u}$	(A6)

Here μ denotes the magnetic permeability (not to be confused with μ_1 used in the main text that denotes the core-fluid viscosity), σ is the electrical conductivity of the medium, $\mathbf{H}$ is the magnetic field, $\mathbf{J}$ is the current and q is the volume charge density in regions where Maxwell's equations are to be solved.

Our interest centers on the possibility of magnetic fields being induced by the AC field that is imposed at the outer electrode, and in particular the effect of the frequency ω. For brevity, we consider such phenomena in the core region 1, since the annular region 2 is taken to be a dielectric, even though this restriction can be lifted in a straightforward manner. Region 1, then, is taken to have permittivity $\epsilon_1 = \epsilon_0 \epsilon_p$, where ϵ_0 is the permittivity of free space, conductivity σ_1 and magnetic permeability $\mu = \mu_0 \mu_p$ where μ_0 is the magnetic permeability of free space. The appropriate time scale is $1/\omega$, and an estimate of the size of $\mathbf{H}$ can be found from the magnetic induction equation (A4); writing $\mathbf{H} = H_0 \mathbf{H}'$ where primes denote dimensionless variables and will be

dropped in due course, and using the scale $E_0 = A/R_0$ for the electric field as in Section II A, gives

$$H_0 = \epsilon_0 \omega E_0 R_0. \tag{A7}$$

Using typical values relevant to the applications of interest here, $\epsilon_0 = 10^{-11}\, F\, m^{-1}$, $R_0 = 10^{-2} cm$ (i.e. a jet of 1cm radius), $E_0 = 10^3\, V\, m^{-1}$, implies that $H_0 \approx 10^{-10}\omega$ Teslas and hence is small and of order 10^{-7} even in the kilohertz range of frequencies (in fact, frequencies in the megahertz range also produce negligible magnetic fields of order $10^{-3}\, T$, in the present problem). Hence, we can ignore the presence of a magnetic field in the model to leading order.

Using (A7) into Faraday's law (A2) yields the dimensionless equation

$$\nabla \times \mathbf{E}' = -(\mu_0 \epsilon_0 \omega^2 R_0)\, \mu_p \frac{\partial \mathbf{H}'}{\partial t'}, \tag{A8}$$

and again an estimate of the term on the right-hand side (using $\mu_0 = 1.257 \times 10^{-6}\, H\, m^{-1}$), provides $\mu_0 \epsilon_0 \omega^2 R_0 \approx 1.257 \times 10^{-19} \omega^2$, which is again negligible for frequencies in the kilohertz and megahertz range. To leading order, therefore, equation (A8) reads

$$\nabla \times \mathbf{E}' = 0, \tag{A9}$$

and hence $\mathbf{E}$ can be expressed as the gradient of a potential in the usual way,

$$\mathbf{E} = -\nabla \phi. \tag{A10}$$

Next we consider the charge conservation equation (A5). Eliminating $\mathbf{J}$ using the charge constitutive law (A6), yields

$$\frac{\partial q}{\partial t} + \mathbf{u} \cdot \nabla q + (\sigma/\epsilon\omega) q = 0, \tag{A11}$$

where we have kept dimensional variables for brevity. It can be seen that along flow characteristics the charge is proportional to $\exp(-\tau_r t)$ where we have introduced the charge relaxation time-scale $\tau_r = (\sigma/\epsilon\omega)$. Using typical values of the conductivity (e.g. de-ionized water) $\sigma = 10^{-6} S\, m^{-1}$, implies $\tau_r \sim 10^5/\omega$ seconds, and if $\omega \ll 10^4\, s^{-1}$, for example, the charge distribution in the bulk becomes zero exponentially fast. As a result, all charge accumulates on the interface and can be computed there using the surface Gauss law (6). This in turn leaves equation (A1) charge-free and coupling this with (A10) along with the fact that ϵ is taken to be constant here, we obtain

$$\nabla^2 \phi = 0. \tag{A12}$$

Equation (A12) is used in modeling electrohydrodynamic problems in the electrostatic limit.

ACKNOWLEDGMENTS

The work of DTP was partly supported by the National Science Foundation grant no. DMS-0707339.

[1] D. Saville, "Electrohydrodynamic stability: effects of charge relaxation at the interface of a liquid jet," J. Fluid Mech., **48**, 815–827 (1971).
[2] A. J. Mestel, "Electrohydrodynamic stability of a highly viscous jet," J. Fluid Mech., **312**, 311–326 (1996).
[3] M. Hohman, M. Shin, G. Rutledge, and M. Brenner, "Electrospinning and electrically forced jets. I. stability theory," Phys. Fluids, **13**, 2201–2220 (2001).
[4] M. Hohman, M. Shin, G. Rutledge, and M. Brenner, "Electrospinning and electrically forced jets. II. applications," Phys. Fluids, **13**, 2221–2236 (2001).
[5] A. Huebner and H. Chu, "Instability and breakup of charged liquid jets," J. Fluid Mech., **49**, 361–372 (1971).
[6] D. Saville, "Stability of electrically charged viscous cylinders," Phys. Fluids, **14**, 1095–1099 (1971).
[7] R. Collins, M. Harris, and O. Basaran, "Breakup of electrified jets," J. Fluid Mech., **588**, 75–129 (2007).
[8] J. M. López-Herrera, P. Riesco-Chueca, and A. M. Gañán Calvo, "Linear stability analysis of axisymmetric perturbations in imperfectly conducting liquid jets," Phys. Fluids, **17**, 1–22 (2005).
[9] J. M. López-Herrera and A. M. Gañán Calvo, "A note on charged capillary jet breakup of conducting liquids: experimental validation of a viscous one-dimensional model," J. Fluid Mech., **501**, 303–326 (2004).
[10] Q. Wang, S. Mahlmann, and D. T. Papageorgiou, "Dynamics of liquid jets and threads under the action of radial electric fields: Microthread formation and touchdown singularities," Phys. Fluids, **21**, 1–19 (2009).
[11] L. Rayleigh, "On the stability of liquid jets," Proc. London Math. Soc., **10**, 4 (1878).
[12] C. Pozrikidis, "Capillary instability and breakup of a viscous thread," J. Eng. Math., **36**, 255–275 (1999).
[13] E. D. Wilkes, S. D. Phillips, and O. A. Basaran, "Computational and experimental analysis of dynamics of drop formation," Phys. Fluids, **11**, 3577–3598 (1999).
[14] D. T. Papageorgiou, "On the breakup of viscous liquid threads," Phys. Fluids, **7**, 1529–1544 (1995).
[15] J. Eggers, "Universal pinching of 3D axisymmetric free-surface flow," Phys. Rev. Lett., **71**, 3458–3460 (1993).
[16] J. Eggers and T. F. Dupont, "Drop formation in a one-dimensional approximation of the Navier-Stokes equation," J. Fluid Mech., **262**, 205–221 (1994).
[17] D. A. Saville, "Electrohydrodynamics: the Taylor-Melcher leaky-dielectric model," Annu. Rev. Fluid Mech., **29**, 27 (1997).
[18] J. M. López-Herrera, A. M. Gañán Calvo, and M. Perez-Sabroid, "One-dimensional simulation of the breakup of capillary jets of conducting liquids. application to e.h.d. spraying," J. Aerosol Sci., **30**, 895–912 (1999).
[19] A. González, F. García, and A. Castellanos, "Stability analysis of conducting jets under ac radial electric fields for arbitrary viscosity," Phys. Fluids, **15**, 395–407 (2003).
[20] S. A. Roberts and S. Kumar, "Ac electrohydrodynamic instabilities in thin liquid films," J. Fluid Mech., **631**, 255–279 (2009).
[21] J. Eggers and E. Villermaux, "Physics of liquid jets," Rep. Prog. Phys., **71** (2008).
[22] J. Eggers, "Nonlinear dynamics and rupture of breakup of free-surface flows," Rev. Mod. Phys., **69**, 865 (1997).
[23] R. V. Craster, O. K. Matar, and D. T. Papageorgiou, "Pinchoff and satellite formation in surfactant covered viscous threads," Phys. Fluids, **14**, 1364 (2002).
[24] P. Keast and P. H. Muir, "Algorithm 688 EPDCOL - a more efficient PDECOL code," ACM Trans. Math. Software, **17**, 153–166 (1991).
[25] Q. Wang, *Nonlinear evolution of annular layers and liquid threads in electric fields* (Ph.D. Thesis, New Jersey Institute of Technology, Newark, New Jersey, 2009).
[26] M. Cloupeau and B. Prunet-Foch, "Electrostatic spraying of liquids in cone-jet mode," Journal of Electrostatics, **22**, 135–159 (1989).
[27] E. Setiawan and S. Heister, "Nonlinear modeling of an infinite

electrified jet," Journal of Electrostatics, **42**, 243–257 (1997).